RSC Advances




ROYAL SOCIETY OF CHEMISTRY

www.rsc.org/advances

RSC Advances

ARTICLE

# Active corrosion inhibition of mild steel by environmentally-friendly Ce-doped organic-inorganic sol-gel coatings

Received 00th January 20xx,
Accepted 00th January 20xx

DOI: 10.1039/x0xx00000x

www.rsc.org/

J. Mosa[a], N. C. Rosero-Navarro[a] and M. Aparicio[a]

The anticorrosive properties of different coatings on mild steel are insufficient and chromate corrosion protection is being eliminated owing to its toxicity. This paper shows an anti-corrosion bi-layer environmentally-friendly sol-gel coating doped with cerium (26 µm thick) on mild steel, combining barrier effect with self-healing. Both layers have a siloxane-methacrylate composition based on the combination of a silicon alkoxide, a monomer and an organically modified silicon alkoxide as a cross-linker. Well-adhered coatings, with excellent barrier properties and current densities as low as $10^{-12}$ A/cm$^2$ and impedances of $10^{10}$ Ohm cm$^2$, are demonstrated. Electrochemical measurements (EIS and polarization tests), SEM-EDX and Micro-Raman analysis indicate depletion of Ce around defects and higher concentration in the defect, supporting the activation of a self-healing process.

## 1. Introduction

Mild steel is the most common type among steels because it combines excellent mechanical properties and a reduced price. Mild steel has low carbon content (up to 0.3%) and it is used where large amounts of steel are necessary, for example in structural applications. However, this steel is very reactive and will revert back to iron oxide when water, oxygen and ions are present. In consequence, there is a demand for low-cost corrosion protection treatments. Some anti-corrosion coatings for protection of mild steel include polyaniline-containing coatings[1-4], polypyrrole coatings[5,6], PVD nitride coatings[7], self-assembled layers of salts[8], etc. On the other hand, chromate in conversion coatings and paints has been used to protect metal substrates (steel and aluminium alloys) against corrosion, because these systems possess the active corrosion inhibition property. However, chromate corrosion protection is being eliminated owing to its high toxicity and carcinogenicity. In consequence, there is increasing demand for the development of chromate-free, environmentally acceptable anti-corrosion pre-treatments.[9,10]

Several inhibitors and coatings are being investigated as alternatives to hexavalent chromium. Transition and rare earth metal ions have been shown to inhibit localized corrosion of aluminium alloys and stainless steels. Cerium ions have emerged as one of the most promising inhibitors for the efficiency shown when it is dissolved in the aggressive solution where the metal substrate is immersed. It is generally accepted that cerium ions dissolved in the electrolyte lead to the precipitation of cerium oxides/hydroxides which delay the cathodic reduction reaction.[11-16]

Sol-gel coatings on metallic substrates have been developed for several decades as barriers facing aggressive electrolytes due to the simplicity in its processing and the chemical bond developed between substrate and coating. Hybrid organic-inorganic sol-gel coatings are being investigated because, in comparison with inorganic coatings, they allow thicker layers with fewer defects and the ability to incorporate corrosion inhibitors. Cerium-doped sol–gel coatings have previously been studied for the corrosion protection of stainless steel, galvanised steel, and Al alloys. However, unlike these 'passive' substrates, mild steel presents a huge challenge for the direct application of a sol–gel coating as the substrate is inherently 'active'. One of the questions that remain unclear is whether the inclusion of cerium into the coating would allow it to work as a corrosion inhibitor in a similar way to it does when is dissolved in the electrolyte. We have demonstrated in this work that cerium ions can diffuse through a porous coating to precipitate as cerium hydroxides/oxides cathodic positions, reducing the corrosion rate by a self-healing process.

Although some studies have shown that cerium nitrate can be doped in a sol–gel coating deposited on mild steel, the system did not result in significant long-term corrosion protection, probably because the cerium, in these circumstances, have difficulties to diffuse and work as a corrosion inhibitor.[17-22] Excellent barrier properties have been demonstrated by siloxane-polymethyl methacrylate hybrid films deposited on carbon steel substrates**.** In the case of un-doped hybrid coatings, $^{29}$Si and $^{13}$C nuclear magnetic resonance (NMR) and thermogravimetric analysis (TGA), as a function of the MMA/MPTS ratio, indicate a high degree of polycondensation (84%) and elevated thermal stability of 410 °C. Doping with cerium ions produces a high degree of connectivity of the network, leading to an enhanced electrochemical stability. The evaluation of the structural effect of cerium revealed that reduction of Ce(IV) ions catalyzes an increase of siloxane network connectivity (>87%) and enhances the polymerization of organic moieties. [23,24] However, the evidences of the inhibition effect of cerium are not clear. Based on our experience in sol-gel silica-methacrylate coatings on aluminium alloys and stainless steel, cerium has to be well distributed in a sol-gel coating with an open structure so that it can diffuse easily. Under these conditions, cerium ions are also

[a] Instituto de Cerámica y Vidrio (CSIC), Kelsen 5, 28049 Madrid, Spain
[b] Address here.
[c] Address here.
† Footnotes relating to the title and/or authors should appear here.
Electronic Supplementary Information (ESI) available: [details of any supplementary information available should be included here]. See DOI: 10.1039/x0xx00000x

easily leached into the electrolyte without reach effectively the corrosion sites; and for this reason it is more useful to combine two different coatings with complementary properties.

Based on these previous results, we demonstrate a thick anti-corrosion bi-layer environmentally-friendly sol-gel coating doped with cerium nitrate on a mild steel substrate. Both layers have a siloxane-methacrylate composition based on the combination of a silicon alkoxide, a monomer and an organically modified silicon alkoxide as a cross-linker for chemical bonding between organic and inorganic components. The protection system combines passive (barrier effect) and active (self-healing process) mechanisms providing efficient corrosion protection in a 3.5 % wt. NaCl solution. Each layer plays a unique role: the inner layer acts as a container for the cerium corrosion inhibitor, with a more open structure to facilitate the diffusion of the cerium ions; and the outer layer acts as a thick highly-condensed barrier against the electrolyte, confining the inhibitor except at flawed points where corrosion processes can appear.

## 2. Experimental section

### 2.1. Synthesis procedure

Two hybrid organic–inorganic sols (un-doped and doped with a cerium salt) were prepared using 3-methacryloxypropyl trimethoxysilane (MPS, ABCR, 98 %), tetraethoxysilane (TEOS, ABCR, 98 %), methyl methacrylate (MMA, Aldrich, 99 %), benzoyl peroxide (BPO, Panreac, 98 %), tetrahydrofuran (THF, Aldrich, 99.9 %), absolute ethanol (EtOH, Panreac, 99.5 %), water ($H_20$, Panreac, 99.9 %), nitric acid ($HNO_3$, Merck, 65 %) and cerium nitrate ($Ce(NO_3)_3{\cdot}6H_2O$, Aldrich, 99%). The un-doped sol, with a molar ratio of MPS:TEOS:MMA:BPO:THF:EtOH:$H_20$ of 1:2:8:0.08:9:20:4, was prepared by mixing two solutions under nitrogen. The first solution was prepared by dissolving BPO in THF and stirring for one hour at room temperature in a reflux flask. Then, MPS was added to the flask (stirring at room temperature), and five minutes later, MMA was added, maintaining the stirring for five minutes. After that, the flask was heated at 70 °C and stirred for 120 minutes. The second solution was prepared by mixing EtOH, TEOS and $H_2O$, as $HNO_3$ 0.1 N, in a reflux flask for 60 minutes at room temperature. Both solutions were mixed at 25 °C and stirred for 30 minutes. The cerium-doped sol was prepared in a similar way, with the same molar ratio of precursors, but the organic polymerization time at 70 °C was reduced to 75 minutes, the stirring time for the second solution to 5 minutes and the stirring time for mixing both solutions to 15 minutes. After that, $Ce(NO_3)_3{\cdot}6H_2O$ was dissolved by stirring, keeping a Si/Ce atomic ratio of 4.3. As a result of the different processing parameters used, the viscosity values for the un-doped sol are about 21 cP, whereas in the case of Ce-doped sol they are around 3.2 cP. The main influence of the different viscosity is the thickness obtained for each coating.

### 2.2. Preparation of coatings

Flat samples of DC01 mild steel (SAE1008) with a nominal composition (wt %) of C≤0.12, Mn≤0.60, P≤0.045 and S≤0.045 were used as substrate. All samples were ultrasonically cleaned with acetone for 15 minutes, rinsed with distilled water and dried with compressed air. The coatings consisted of an inner layer prepared with the Ce-doped sol and an outer layer prepared with the un-doped sol. In the case of the Ce-doped layer, the deposition was performed by dipping at a withdrawal rate of 14.3 cm $min^{-1}$, leaving it to dry at room temperature for 20 minutes. This procedure was repeated four times, and then, the samples were heat-treated at 60 °C (1 °C $min^{-1}$) for 48 hours and 160 °C (1 °C $min^{-1}$) for 5 hours.[23] After the deposition of each layer the coating has a gel texture, so the deposition of the successive layers at room temperature does not produce an interface between layers. The final thermal treatment consolidates the five-layer coating as it was only one layer. The outer layer (un-doped) was also prepared by dipping using the same experimental procedure.

### 2.3. Structural and mechanical characterization

Characterization of the coatings included the analysis of the surface and cross-section of coated samples through scanning electron microscopy (HITACHI S-4700 field emission) and elemental chemical analysis through Energy Dispersive X-ray Spectroscopy (EDX, NORAN system six). A post-mortem analysis of coated samples after electrochemical evaluation was also performed using this equipment. Compositional depth profiling of the coated metal substrate was obtained using a ToF-SIMS[5] (Time of Flight Secondary Ions Mass Spectrometer) Ion Tof. A pulsed 25 KV $Bi_3^{++}$ ion source was employed for analysis over a 21.9 x 21.9 µm area. Sputtering was performed using a 2 kV oxygen beam over a 250 x 250 µm area. Data acquisition and post-processing analyses were carried out using Ion-Spec software. Micro-scratch tests were performed on coated substrates operating in ''progressive load'' mode (Model APEX-1, CETR equipment), using a conical type diamond with 5 µm tip radius, 1.2 mm/min sliding speed, 5 to 200 mN incremental normal load and 2 mm scratch pattern. Normal and tangential forces were recorded, and scanning electron microscopy (HITACHI S-4700 field emission) was used to examine the morphology of the residual scratch patterns. The Raman study was carried out using a Confocal Micro-Raman (CRM) coupled with AFM (Witec alpha-300R). Spectra were obtained using a frequency doubled Nd-YAG laser operating at 532 nm and an x100 objective lens (NA = 0.9). The incident laser power was 35 mW and the Raman spectral resolution was down to 0.02 $cm^{-1}$. The sample was mounted on a piezo-driven scan platform with 4 nm lateral and 0.5 mm vertical positional accuracy. The piezoelectric scanning table allows steps of 3 nm (0.3 nm in the vertical direction), giving a very high spatial resolution for both the AFM and the CRM. Collected spectra were analysed using Witec Control Plus Software.

### 2.4. Electrochemical characterization

Electrochemical assays were conducted on coated and uncoated substrates in a three electrode cell in 3.5 wt.% NaCl solution at room temperature with a saturated calomel electrode (SCE) as the reference electrode, a platinum mesh of convenient area as the counter electrode and the test coupons as the working electrode. Assays were carried out in an electrochemical unit (Multichannel Potentiostat VMP3 from Bio-Logic SAS). Potentiodynamic polarization curves were recorded from -0.050 V to +1.500 V vs corrosion potential (Ecorr) at a scan rate of 0.6 V $h^{-1}$ (ASTM G 59). Electrochemical impedance spectroscopy (EIS) was performed with sweeping frequencies from 20,000 to $10^{-3}$ Hz and modulating 0.020 V (rms) around Ecorr. Impedance fitting was performed using Bio-Logic software. Electrochemical tests were performed following a specific configuration: 1) a succession of tests including potential measurement, potentiodynamic polarization and impedance analyses as a function of the immersion time until a clear signal of degradation of the barrier properties of the coating system appears

(induction of a defect); and 2) after that, a new series of tests in the same tested area, including only successive potential measurements combined with impedance analysis as a function of the immersion time. The object was to study the durability of the barrier effect, and then the evaluation of the corrosion inhibition provided by the cerium ions.

## 3. Results and discussion

### 3.1. Cross-section characterization

Optimized solutions made it possible to obtain homogeneous transparent coatings on the mild steel substrate, which were yellowish in the case of Ce-doped coatings. Figure 1 presents a cross-section SEM micrograph of a coated sample, showing homogeneous layers. The thickness of the inner Ce-doped and outer un-doped layers are around 3.1 and 22.9 µm, respectively. This significant difference in thickness comes from the different viscosity values of the solutions, because both parameters are interrelated in the dipping process. The identification of the different layers is confirmed by EDX analysis, also shown in Figure 1, indicating that both coatings contain mainly silicon and carbon; and only the inner one also cerium.

Figure 2 displays the ToF-SIMS depth profiles of the bi-layer coating on the mild steel. The location of the coating – metal substrate interface can be approximately determined by the intersection of the $Fe^+$ line with the $Si^+$ and $CeO^+$ lines. The significant increase in intensity observed when sputtering approaches the interface between the un-doped and Ce-doped

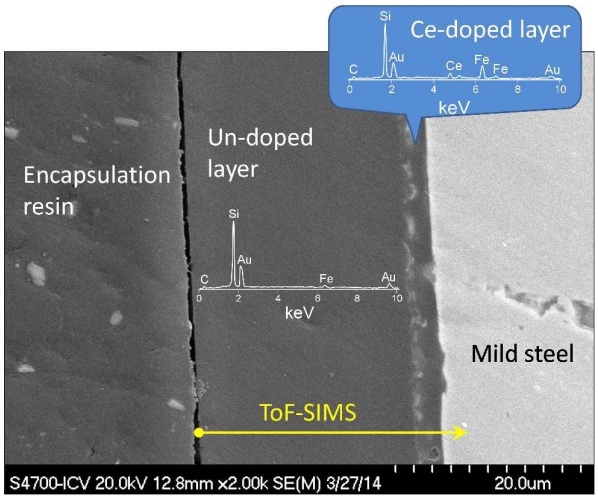


Fig. 1. Scanning Electron Microscopy (SEM) micrograph including Energy Dispersive X-ray Spectroscopy (EDX) of the coated steel substrate (both layers).

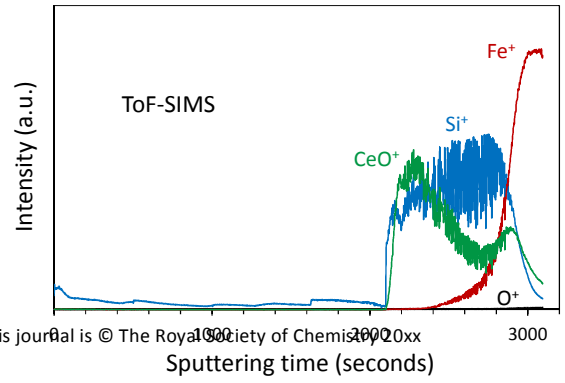


Fig. 2. ToF-SIMS (Time of Flight Secondary Ions Mass Spectrometer) depth profiles of the coated steel substrate.

layers is the result of increased conductivity due to the presence of cerium and the metal substrate itself. The resulting sputtering time is consistent with the microscopic observations, showing a thick coating for the outer un-doped layer in comparison with the Ce-doped layer.

### 3.2. Micro-scratch tests

An important property for an efficient corrosion protection coating is strong adhesion, able to maintain integrity even during the penetration of the electrolyte. For this reason, an analysis of the adhesive behaviour of the coating is necessary.
Figure 3a presents the normal load applied ($F_z$) and tangential force ($F_x$) as a function of the horizontal displacement (Y) after a progressive load scratch test with a 5 µm tip radius indenter. The frictional forces between the scratch probe and surface of the material can be expressed by $F_x/F_z$. The trend of the tangential force profile shows two different steps: a first step with a linear ascent at low load, and then a serrated line shape increasing in intensity at moderate and high loads. The boundary point between the two branches, where the first

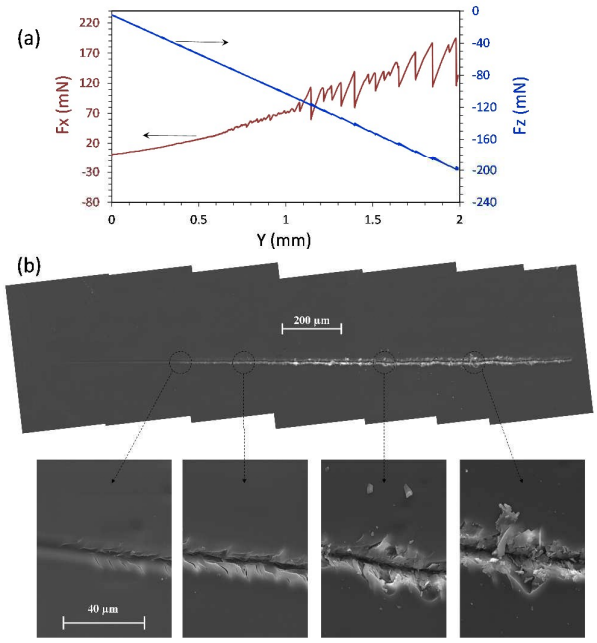


Fig. 3. Micro-scratch tests on the coated substrate operating in ''progressive load'' mode: a) Normal ($F_z$) and tangential ($F_x$) forces versus horizontal displacement (Y); b) Scanning Electron Microscopy (SEM) micrographs at different magnifications of the residual scratch pattern.

variations of $F_x$ can be observed, can be located at a horizontal displacement of 0.66 mm from the beginning of the scratch. This value indicates a critical load of 70.3 mN (normal load applied). This critical load defines the minimal load for the occurrence of a failure

event in the coating, which could mean detachment of the coating or only a significant deformation of a well-adhered layer. From a horizontal displacement larger than 1.05 mm the variations of $F_x$ are higher, which is associated with some fragments of the coating being removed. Figure 3b displays the residual scratch patterns at low and high magnifications, showing plastic deformation behaviour. In addition, several linear cracks propagate along a 45° direction toward the sides of the scratch pattern. The micrographs confirm the critical load, calculated using the force-displacement plot, to produce the failure of the coating. As the load increases, it can be observed how some fragments are removed but without delamination of the coating. This ductile deformation under the advancing indenter and the excellent adhesion observed are two important properties to obtain good corrosion-resistant coatings.[25]

### 3.3. Electrochemical evaluation of bi-layer coated substrates (up to 354 days of immersion)

In order to compare the susceptibility of the coated system to corrosion with the uncoated metal, anodic polarization and impedance curves were recorded. Literature shows good barrier properties without self-healing effect for siloxane-polymethyl methacrylate hybrid films, and low long-term corrosion protection when these coatings are doped with cerium.[12,14,23,24]

Figure 4 shows polarization curves of the bare and coated material after increasing immersion time in 3.5 wt. % NaCl solution at room temperature on the same test area. The bare mild steel shows active dissolution during the first day of immersion, while the coated material shows excellent corrosion protection efficiency. After one day of immersion in NaCl solution, the coated substrate shows very low current densities, around seven orders of

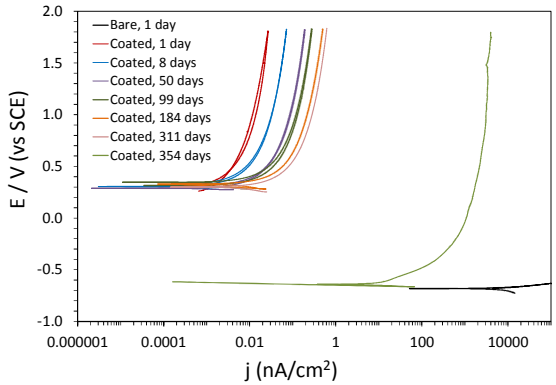


Fig. 4. Potentiodynamic polarization curves of the bare and coated steel substrate after increasing immersion time in 3.5 wt. % NaCl solution on the same test area up to 354 days of immersion.

magnitude lower than those of the bare substrate. The coating seems to remain unaltered during polarization, suggesting a very stable superficial film without any breakdown potential (potential in which passivity breaks and current density increases in a monotonic way with potential) at this stage. Detailed analyses indicated that the inorganic phase plays an important role in promoting adhesion between the coating and the metal substrate, while the organic phase hermetically seals the film structure.[23,26,27]

Increasing immersion time to 311 days leads to a slow rise in the current density reached at maximum potential, but only in approximately one order of magnitude. This behaviour can be associated with some kind of degradation of the coatings, although this should be insignificant because the current density is very low, the corrosion potential does not change and there are no signs of breakdown potential. The polarization curve after 354 days of immersion shows a very different tendency because the corrosion potential is now close to that of bare substrate. This value, together with the reduction of current density, is associated with some degradation of the coating system. However, the absence of breakdown potential indicates that this degradation is limited. At this point, it is not possible to determine whether the presence of cerium ions in the coating is at least partially responsible for this excellent performance, or is merely a consequence of the good barrier performance of this coating system.

In order to analyse the polarization results in more detail, impedance measurements were carried out after each polarization curve. Figure 5 displays Bode plots (log/Z/ vs. log frequency and phase angle vs. log frequency) for the coated substrate for different immersion times, and the comparison with the bare steel during the first day of immersion in NaCl solution. The open circuit potential values (shown on the plot) are the first indication of the system response trend during immersion: positive values around +0.35 V for a defect-free coating and a negative value (-0.56 V), close to that of the bare substrate, only when some degradation appears after 354 days. Bare material shows two time constants in the phase plot suggesting that the system response could be related to metal corrosion and the presence of an oxide formed on the steel. The system response for the coated steel after immersion times of up to 354 days is highly capacitive in the frequency domain under study, showing only one time constant. This behaviour corresponds to a homogeneous defect-free coating. Impedance values at 1 mHz are around $10^{10}$ Ohm, six orders of magnitude higher than that of the bare substrate, according to the polarization

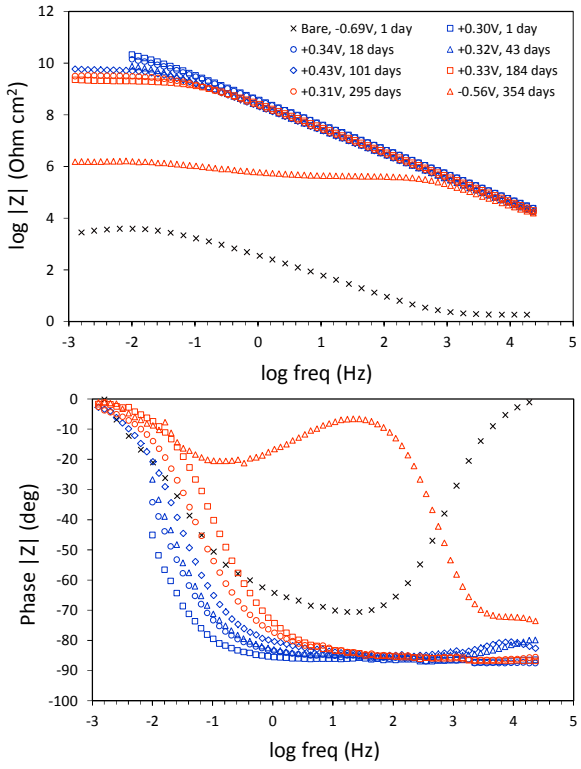


Fig. 5. Electrochemical Impedance Spectroscopy (EIS) of the bare and coated steel substrate after increasing immersion time in 3.5

wt. % NaCl solution on the same test area up to 354 days of immersion.

results. This impedance value decreases slowly with the immersion time, following the same tendency observed in polarization tests. After 354 days of immersion, a downturn is observed on both the impedance and phase angle plots, which could be associated with the penetration of the electrolyte in the coating. Again, this behaviour follows the trend observed in the polarization test. In this case (354 days of immersion), the system response can be composed of three different contributions: the one at higher frequencies ($10^4$ Hz) associated with the coating response; the second one at medium frequencies (1 Hz) related to the oxide formed on the metal substrate; and the last one in the low frequency region ($10^{-1}$ Hz) corresponding to the corrosion of the metal substrate. The electrochemical behaviour can be described in terms of an equivalent circuit in order to provide the most relevant parameters applicable to the corroding system (Table 1). A constant phase element (CPE) was used instead of an ''ideal'' capacitor, taking into account that the slopes on the curves in the log |Z| vs. log freq. plot were not 1 (value expected for an ideal capacitor) and certain degree of inhomogeneity on the surface. The equivalent circuits shown in the table were used for the bare and coated substrates, and consist of the following elements: $R_s$ represents the electrolyte resistance, $CPE_{coat}$ is related with the non-ideal capacitance of the coating, $R_{coat}$ is the resistance presented by the pores or defects to the passage of the electrolyte, $CPE_{ox}$ is the constant phase element related to the oxide formed on the steel, $R_{ox}$ corresponds to the oxide resistance, $CPE_{dl}$ considers the presence of a double layer between the metal surface and the electrolyte e.g.: $CPE_{dl}$ is related to the non-ideal capacitance of the

Table 1. Equivalent circuits and fitting parameters for the impedance measurements plotted in Figure 5.

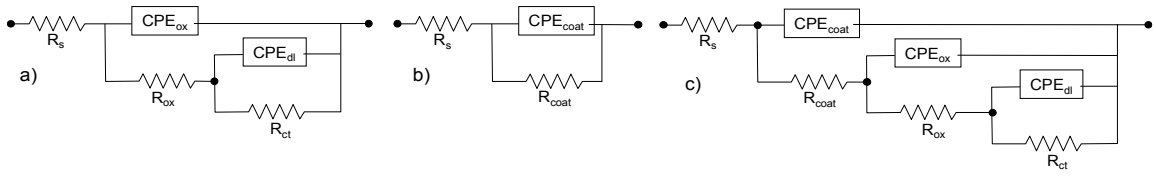


| | $R_s$/Ωcm$^2$ | $R_{coat}$/Ωcm$^2$ | $CPE_{coat}$ | | $R_{ox}$/Ωcm$^2$ | $CPE_{ox}$ | | $R_{ct}$/Ωcm$^2$ | $CPE_{dl}$ | |
|---|---|---|---|---|---|---|---|---|---|---|
| | | | $C_{coat}$/Fcm$^{-2}$s$^{a-1}$ | a | | $C_{ox}$/Fcm$^{-2}$s$^{a-1}$ | a | | $C_{dl}$/Fcm$^{-2}$s$^{a-1}$ | a |
| Bare, 1 day (a) | 2.36 | | | | 4.72 E+02 | 3.06 E-04 | 0.87 | 4.85 E+03 | 2.86 E-04 | 0.71 |
| Coated, 1 day (b) | 30 | 3.97 E+10 | 0.35 E-09 | 0.96 | | | | | | |
| Coated, 18 days (b) | 30 | 2.06 E+10 | 0.38 E-09 | 0.95 | | | | | | |
| Coated, 43 days (b) | 30 | 1.12 E+10 | 0.63 E-09 | 0.94 | | | | | | |
| Coated, 101 days (b) | 30 | 7.10 E+09 | 0.67 E-09 | 0.93 | | | | | | |
| Coated, 184 days (b) | 30 | 2.53 E+09 | 0.50 E-09 | 0.95 | | | | | | |
| Coated, 295 days (b) | 30 | 4.01 E+09 | 0.62 E-09 | 0.94 | | | | | | |
| Coated, 354 days (c) | 30 | 5.05 E+05 | 1.29 E-09 | 0.90 | 3.60 E+03 | 0.72 E-09 | 0.94 | 1.73 E+06 | 0.99 E-06 | 0.64 |

double layer, and $R_{ct}$ is related to the charge transfer resistance of the metal. This table also shows the fitting of the data for the equivalent circuits. Errors from numerical fitting were always below 10 %. The values of $R_{coat}$ and $CPE_{coat}$ do not show any significant change with immersion time of up to 354 days, confirming the excellent corrosion protection efficiency of the coating. The results of the sample after 354 days of immersion show a significant reduction of $R_{coat}$ (four orders of magnitude). The presence of two new time constants at low frequency can be assigned to an increase in the area of metal exposed and electrolyte penetration in the coating through the cracks and pores. However, the $C_{coat}$ value only increased a little, indicating that the coating remains almost intact. Consequently, $R_{ct}$ and $CPE_{dl}$ values differ by three orders of magnitude compared to the bare substrate. At this point, the impedance analysis shown so far does not present any indication of an active corrosion inhibition process, only a very slow degradation of a barrier system.

### 3.4. Electrochemical evaluation of bi-layer coated substrates (above 354 days of immersion)

After this sequence of polarization-impedance tests, which led to partial degradation of the protection system, a new series of tests combining potential and impedance measurements (maintaining the immersion of the same test area) were carried out to study the presence of a self-healing effect on a system that already has some kind of partial damage. Figure 6 shows the variation of corrosion potential with immersion time, whereas zero time on the plot corresponds to the end of the polarization-impedance measurements performed during 354 days of immersion. The potential curve shows gaps at different time ranges corresponding to the impedance measurements performed. The impedance tests, marked with their number on the plot, are shown in Figure 7. Considering the high concentration of sodium chlorate in the solution, the significant variation in the potential values at different times is very interesting as they change from negative values around -0.60 V, very close to the bare material, to positive values about +0.20 V, similar to those obtained initially for crack-free coatings. This behaviour may be related to an active corrosion inhibition process provided by cerium ions present in the coating. After some time of high stable potential, a reduction to negative

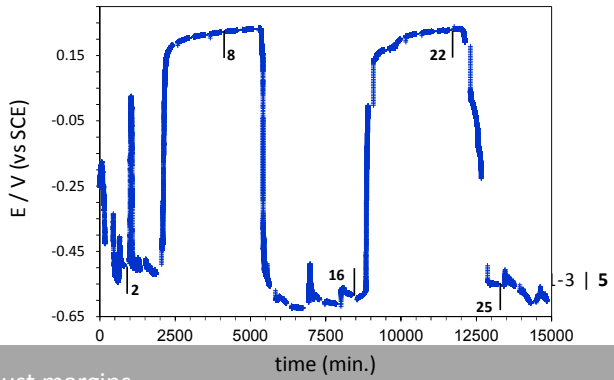

Fig. 6. Corrosion potential versus immersion time of the coated steel substrate after increasing immersion time in 3.5 wt. % NaCl solution on the same test area after the polarization-impedance measurements made during 354 days of immersion.

values can be associated once again with the activation of the corrosion process. For the second time, the self-healing process is triggered, generating a further increase in potential.

In order to analyse this process in detail, the impedance measurements (Bode plots) indicated on the potential-time plot are shown in the Figure 7.

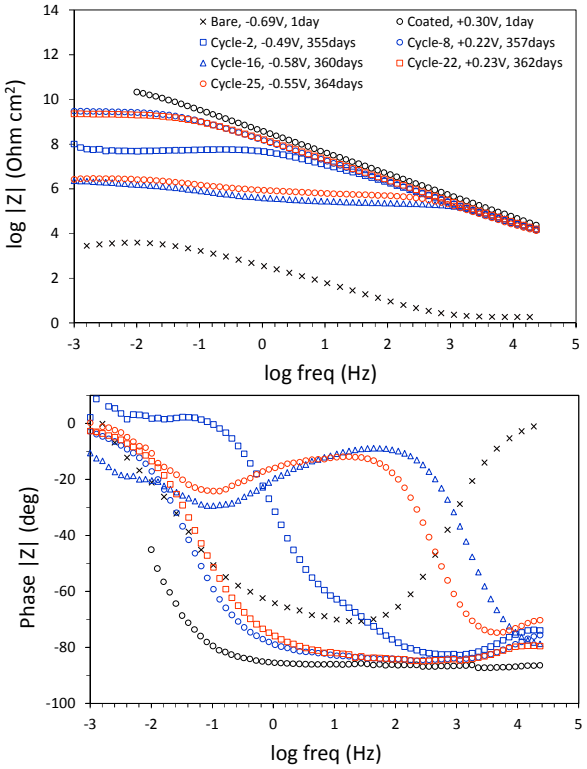


Fig. 7. Electrochemical Impedance Spectroscopy (EIS) of the bare and coated steel substrate after increasing immersion time in 3.5 wt. % NaCl solution on the same test area after the polarization-impedance measurements made during 354 days of immersion.

The measurements for the bare and coated substrate after one day of immersion are also included in the figure for comparison. Even at first glance, two different type of behaviour can be observed: curves with high total impedance values (almost $10^{10}$ Ohm $cm^2$) and positive values of corrosion potential, and curves with lower impedance values (almost $10^7$ Ohm $cm^2$) and negative values of corrosion potential, close to that of bare mild steel. The system response for the first group is highly capacitive, showing only one time constant associated with a homogeneous defect-free coating. The second group of curves shows more than one time constant related to the coating properties, corrosion process and, probably, the corrosion inhibition provided by cerium ions. The decrease in the phase angle in the high frequency region together with a reduction in the impedance modulus denotes deterioration in the coating system. An intermediate case is the test performed immediately after completion of the combined polarization-impedance trials of the previous stage (Cycle-2, 355 days of immersion). Signs of the corrosion inhibition process are the increase in both the impedance modulus and the corrosion potential after partial degradation of the system response, indicated by a reduction in the values of impedance and corrosion potential. The usual behaviour of a sol-gel coating protecting a metal substrate is the continuous degradation of the system response due to a reduction in total impedance with immersion time. The fitting of the impedance results to equivalent circuits confirms the activation of a self-healing process (Table 2).

This table shows the equivalent circuits and fitting of the EIS results from Figure 7. Errors from numerical fitting were always lower than 10 %. The $R_{coat}$ values clearly show the trend mentioned above, and impedance values corresponding to an almost intact coating and impedance values related to a coating with partial degradation can be seen. The difference between both types of behaviour produces a difference of 4 orders of magnitude in the impedance values. This different behaviour does not affect the $CPE_{coat}$ values, which do not present any significant changes, indicating that the partial degradation of the coating system after the prolonged immersion is small. The curves with lower total impedance values (Cycles 16 and 25) present two additional time constants associated with a thin layer of oxide on the metal surface ($R_{ox}$-$CPE_{ox}$) and the charge transfer process ($R_{ct}$-$CPE_{dl}$). In both curves, the resistance values are quite high, $10^5$ and $10^6$ Ωcm$^2$, respectively, confirming the excellent protection efficiency. The intermediate case (Cycle 2) does not clearly show the presence of the time constant related to the corrosion process because it should be minimal in view of the $R_{coat}$ and $R_{ox}$ values, but enough to trigger the self-healing mechanism.

Table 2. Equivalent circuits and fitting parameters for the impedance measurements plotted in Figure 7.

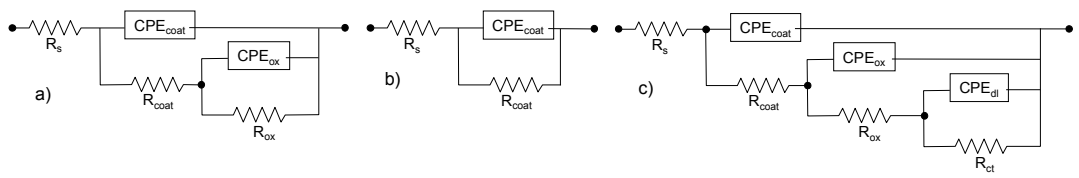


| | $R_s$/Ωcm$^2$ | $R_{coat}$/Ωcm$^2$ | $CPE_{coat}$ | | $R_{ox}$/Ωcm$^2$ | $CPE_{ox}$ | | $R_{ct}$/Ωcm$^2$ | $CPE_{dl}$ | |
|---|---|---|---|---|---|---|---|---|---|---|
| | | | $C_{coat}$/Fcm$^{-2}$s$^{a-1}$ | a | | $C_{ox}$/Fcm$^{-2}$s$^{a-1}$ | a | | $C_{dl}$/Fcm$^{-2}$s$^{a-1}$ | a |
| Cycle-2, 355 days (a) | 30 | 3.12 E+07 | 1.16 E-09 | 0.91 | 3.82 E+07 | 1.02 E-09 | 0.91 | | | |
| Cycle-8, 357 days (b) | 30 | 3.65 E+09 | 0.99 E-09 | 0.92 | | | | | | |
| Cycle-16, 360 days (c) | 30 | 2.69 E+05 | 0.67 E-09 | 0.94 | 6.18 E+05 | 1.04 E-06 | 0.51 | 2.43 E+06 | 4.45 E-07 | 0.86 |
| Cycle-22, 362 days (b) | 30 | 2.72 E+09 | 0.90 E-09 | 0.92 | | | | | | |
| Cycle-25, 364 days (c) | 30 | 7.11 E+05 | 1.58 E-09 | 0.89 | 3.38 E+05 | 1.03 E-07 | 0.93 | 2.89 E+06 | 9.15 E-07 | 0.69 |

The sample was removed from the test cell, cleaned and dried at room temperature. The surface of the coating remained almost intact, and only a few small cracks were found (Figure 8). This crack seems to appear around an inhomogeneity, probably on the metal

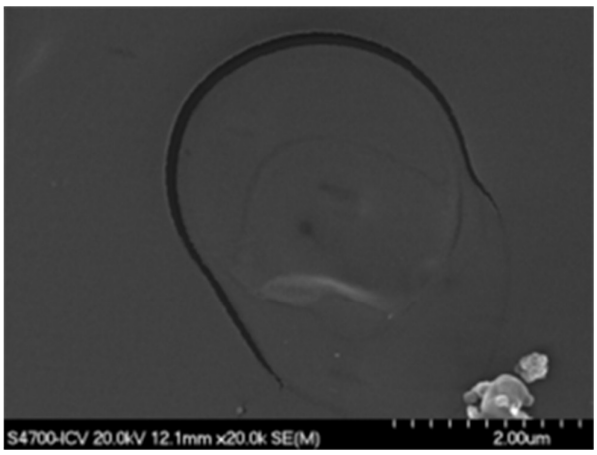


Fig. 8. Scanning Electron Microscopy (SEM) micrograph of the coating after electrochemical measurements in 3.5 wt. % NaCl solution during 364 days of immersion.

surface, and was produced during the prolonged immersion and the sequence of anodic polarizations performed. Considering the coating thickness of this bi-layer system, the mechanism of corrosion inhibition provided by the cerium ions could not be studied by SEM-EDX to confirm the self-healing signals observed in the electrochemical results.

### 3.5. Coating mechanism

Consequently, a mild steel substrate protected only with the inner Ce-doped layer was immersed in 3.5 wt. % NaCl solution for one month. Figure 9a presents a defect on the surface of the Ce-doped layer after the immersion in 3.5 wt. % NaCl solution. The EDX analysis (Figure 9b) shows a significant increase in cerium concentration at the bottom of the defect, already on the metal surface. The semi-quantitative calculations indicate Si/Ce rates (% atom) of 2.9 and 12.2 for the analysis performed at the bottom of the defect and layer surface, respectively. These results clearly indicate a depletion of Ce around the defect and an increase in its concentration at the bottom of the defect in relation to the nominal quantities (Si / Ce = 4.3), which would support an active corrosion inhibition process. This post-mortem study was conducted only on the Ce-doped layer. Given the bi-layer system and the good properties displayed as a barrier, the accessible metal area would be very limited and the efficiency of the Ce-doped layer would be much higher. In this sense, the presence of defects would activate the corrosion process, triggering the diffusion of cerium ions in the electrolyte inside the defect, and then the precipitation of cerium hydroxide-oxide on cathodic sites, "healing" the defect at this location and increasing the corrosion potential (Figure 10).

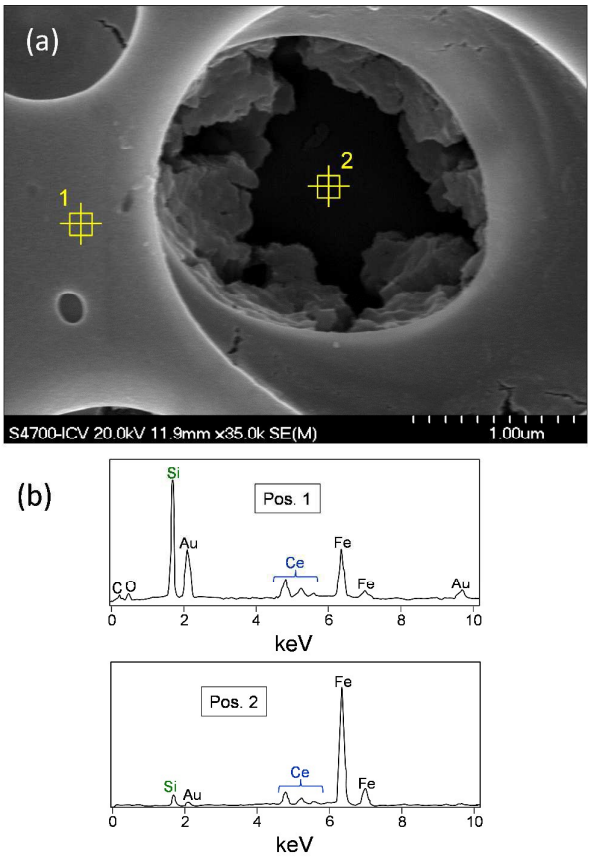


Fig. 9. Analysis of a substrate protected only with the inner Ce-doped layer after one month of immersion in 3.5 wt. % NaCl solution: a) Scanning Electron Microscopy (SEM) micrograph of the coating surface showing a defect; b) Energy Dispersive X-ray Spectroscopy (EDX) plots for the coating surface and inside the defect.

Following the analysis of the corrosion inhibition by self-healing, a post-mortem study was carried out using Confocal Micro-Raman (CRM) coupled with AFM on a substrate protected with the bi-layer system after immersion in 3.5 wt. % NaCl solution. The comparison of the spectra obtained outside and inside the tested area (Figure 11) indicates that both are almost identical and there is no evidence of corrosion products. No remarkable changes were observed, indicating high chemical stability of the hybrid network during the corrosion analysis. The results also show that a hybrid network was formed through the bonding of organic and inorganic components. The band at 1140 $cm^{-1}$ was assigned to C-O-C and Si-O-C groups, meaning that the organic precursor was bonded with MPS and TEOS.[28] The intensity of the carbonyl stretching frequency (1752 $cm^{-1}$) increased in the hybrid coating as compared to pure MMA monomer (1727 $cm^{-1}$), which indicates the presence of an interaction between MMA and $SiO_2$.[29]

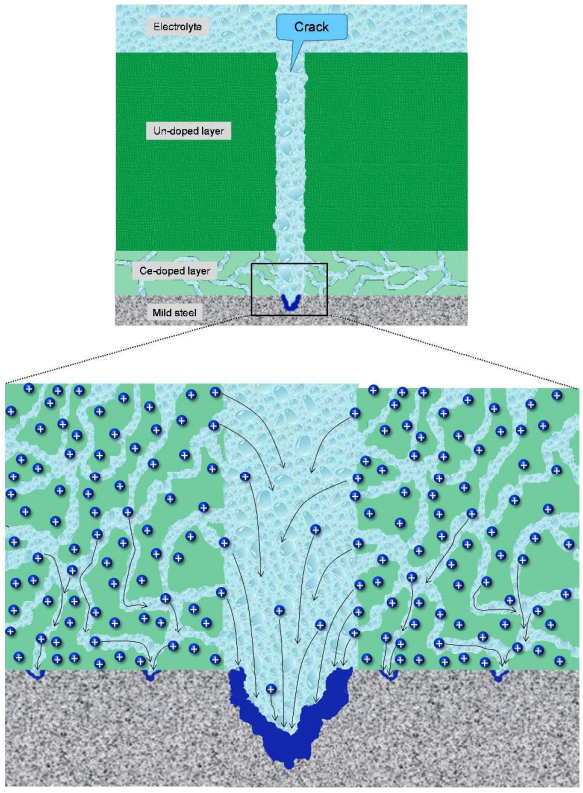


Fig. 10. Diagram of the active corrosion inhibition mechanism from self-healing after a defect is induced in the coating system. The activation of the corrosion process triggers the diffusion of cerium ions towards the points of corrosion, precipitating as hydroxide-oxides.

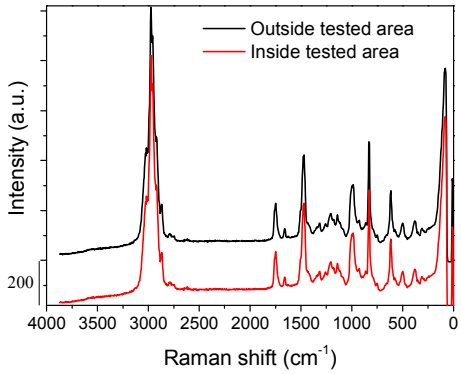


Fig. 11. Raman spectra at a depth of 10 µm (inside the un-doped layer) of the coated steel substrate after the immersion in 3.5 wt. % NaCl solution. The selected areas, outside and inside the tested area, were 10 µm x 10 µm. The acquisition time was 3.6 seconds for one single spectrum and the Raman image consists of 3000 spectra.

A 532 nm excitation wavelength was used to acquire x-z-Raman depth profiles. These profiles were collected employing the x-z-scan modus starting the analysis in the upper layer of the protection system (un-doped coating), then going down to the Ce-doped, and finishing at the substrate-coating interface. First, AFM confocal microscopy was used to select a region inside the corroded area with a defect (Figure 12a).

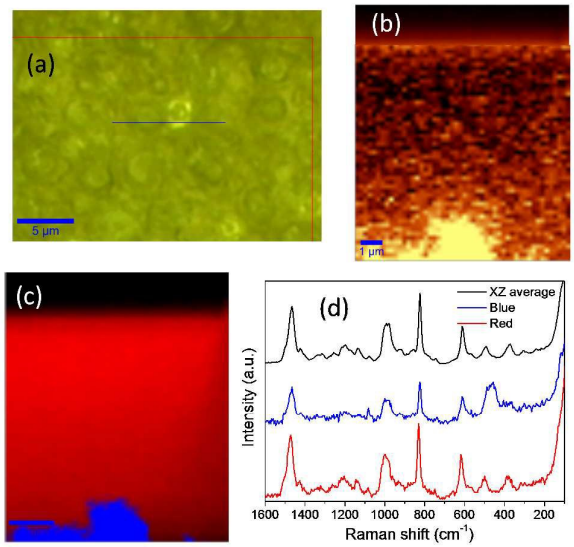


Fig. 12. Confocal Micro-Raman (CRM) coupled with AFM analysis of the coated substrate after the immersion in 3.5 wt. % NaCl solution: a) AFM confocal microscopy image at around 24 µm (inside Ce-doped layer) showing the line for analysis; b) XZ Raman depth scan image corresponding to this line. The deeper yellow is associated with the cerium band (466 $cm^{-1}$); c) Raman image (integration time of 0.03 sec). The colours in the spectra correspond to different areas in the Raman image using a filter for 466 $cm^{-1}$. Scale bar: 20 µm; d) Main Raman spectra associated with the two different colours, and average spectra for comparison.

This image corresponds to a depth of around 24 µm (inside Ce-doped layer), showing the area (line) to be analysed vertically above and below. To distinguish the components of the coating (Figure 12b), the different images generated by the fit procedure were illustrated with different colours and combined in one Raman image (Figure 12c). The presence or absence of cerium hydroxide was detected by the strong band at 466 $cm^{-1}$, corresponding to an $F_{2g}$ Raman band from the space group *Fm3m* in a cubic fluorite structure (Figure 12d).[30-32] This peak could be due to the existence of a large amount of oxygen vacancies (mixture of $Ce^{4+}$ and $Ce^{3+}$ ions) in the deposited cerium hydroxide layer. The Raman images clearly reveal that cerium compounds were mainly present at the bottom of the coating in the interface with the substrate.

## 4. Conclusions

The siloxane-methacrylate bi-layer coating combines a barrier effect with self-healing, providing efficient protection of mild steel in NaCl solution. Both layers have a hybrid network based on the combination of a silicon alkoxide, a monomer and an organically modified silicon alkoxide as a cross-linker for chemical bonding between organic and inorganic components. Each layer plays a unique role: the inner layer (3.1 µm) acts as a container for the cerium corrosion inhibitor, with a more open structure to facilitate the diffusion of the cerium ions; and the outer layer (22.9 µm) acts as a thick highly-condensed barrier against the electrolyte,

confining the inhibitor except at flawed points where corrosion processes can appear. The micro-scratch tests indicate a ductile deformation under the advancing indenter and a good adhesion of the coating. Electrochemical measurements show a coating with excellent barrier properties and very low current densities. After a year of an ongoing series of polarization and impedance measurements, the switching between high impedance values with positive potentials and lower impedance values with negative potentials is associated with active corrosion inhibition. SEM-EDX and Micro-Raman analyses indicate depletion of Ce around defects and higher concentration in the defect, supporting the activation of a corrosion inhibition process. These results demonstrate the diffusion of cerium ions that precipitate into corrosion areas, triggering a self-healing mechanism. It is apparent that cerium ions performed as a highly effective corrosion inhibitor within the sol–gel coating.

## Acknowledgements

This work was backed by the Ministerio de Economía y Competitividad (Spain), programme PCIN-2013-030. We are grateful to M. Gómez, L. Peláez, D. Ruiz, Dr D. Soriano and Dr A. del Campo for their support with laboratory techniques.

## Notes and references

1 F. Chen and P. Liu, *ACS Appl. Mater. Interfaces*, 2011, **3**, 2694.
2 Di Chu, Jixiao Wang, Yufeng Han, Qiang Ma and Zhi Wang, *RSC Adv.*, 2015, **5**, 11378.
3 Wei-Kang Lu, Ronald L. Elsenbaumer and Bernhard Wessling, *Synthetic Metals*, 1995, **71**, 2163.
4 P. Li, T.C. Tan and J.Y. Lee, *Synthetic Metals*, 1997, **88**, 237.
5 P. Ocón, A.B. Cristobal, P. Herrasti and E. Fatas, *Corros. Sci.*, 2005, **47**, 649.
6 J. Reut, A. Öpik and K. Idla, *Synthetic Metals*, 1999, **102**, 1392.
7 C. Liu, A. Leyland, Q. Bi and A. Matthews, *Surf. Coat. Technol.*, 2001, **141**, 164.
8 H.N. Shubha, T.V. Venkatesha, K. Vathsala, M.K. Pavitra and M.K. Punith Kumar, *ACS Appl. Mater. Interfaces*, 2013, **5**, 10738.
9 J.H. Osborne, *Prog. Org. Coat.*, 2001, **41**, 280.
10 D.G. Barceloux, *J. Toxicol. Clin. Toxicol.*, 1999, **37**, 173.
11 M. Mouanga, F. Andreatta, M.E. Druart, E. Marin, L. Fedrizzi and M.G. Olivier, *Corros. Sci.*, 2015, **90**, 491.
12 N.C. Rosero-Navarro, M. Curioni, Y. Castro, M. Aparicio, G.E. Thompson and A. Durán, *Surf. Coat. Technol.*, 2011, **206**, 257.
13 M. Garcia-Heras, A. Jimenez-Morales, B. Casal, J.C. Galvan, S. Radzki and M.A. Villegas, *J. Alloys Compd.*, 2004, **308**, 219.
14 N.C. Rosero-Navarro, S.A. Pellice, A. Durán and M. Aparicio, *Corros. Sci.*, 2008, **50**, 1283.
15 M. Bethencourt, F.J. Botana, J.J. Calvino, M. Marcos and M.A. Rodríguez-Chacón, *Corros. Sci.*, 1998, **40**, 1803.
16 B.R.W. Hinton, *J. Alloys Compd.*, 1992, **180**, 15.
17 H. Wang and R. Akid, *Corros. Sci.*, 2008, **50**, 1142.
18 I. Santana, A. Pepe, E. Jimenez-Pique, S. Pellice and S. Ceré, *Surf. Coat. Technol.*, 2013, **236**, 476.
19 I. Santana, A. Pepe, E. Jimenez-Pique, S. Pellice, I. Milošev and S. Ceré, *Surf. Coat. Technol.*, 2015, **265**, 106.
20 A. Phanasgaonkar and V.S. Raja, *Surf. Coat. Technol.*, 2009, **203**, 2260.
21 W. Trabelsi, P. Cecilio, M.G.S. Ferreira and M.F. Montemor, *Prog. Org. Coat.*, 2005, **54**, 276.
22 W. Trabelsi, E. Triki, L. Dhouibi, M.G.S. Ferreira, M.L. Zheludkevichc and M.F. Montemor, *Surf. Coat. Technol.*, 2006, **200**, 4240.
23 P. Hammer, F.C. dos Santos, B.M. Cerrutti, S.H. Pulcinelli and C.V. Santilli, *J. Sol-Gel Sci. Technol.*, 2012, **63**, 266.
24 S.V. Harb, F.C. dos Santos, B.L. Caetano, S.H. Pulcinelli, C.V. Santilli and P. Hammer, *RSC Adv.*, 2015, **5**, 15414.
25 M. Barletta, A. Gisario, M. Puopolo and S. Vesco, *Mater. Design*, 2015, **69**, 130.
26 S.V. Harb, B.M. Cerrutti, S.H. Pulcinelli, C.V. Santilli and P. Hammer, *Surf. Coat. Technol.*, 2015, **275**, 9.
27 V.H.V. Sarmento M.G. Schiavetto, P. Hammer, A.V. Benedetti, C.S. Fugivara, P.H. Suegama, S.H. Pulcinelli and C.V. Santilli, *Surf. Coat. Technol.*, 2010, **204**, 2689.
28 D. Fischer, D. Pospiech, U. Scheler, R. Navarro, M. Messori and P. Fabbri, *Macromol. Symp.*, 2008, **265**, 134.
29 K.J. Thomas, M. Sheeba, V.P.N. Nampoori, C.P.G. Vallabhan and P. Radhakrishnan, *J. Opt. A: Pure Appl. Opt.*, 2008, **10**, 055303.
30 Q.F. Han, L. Chen, F. Qiang, W.C. Zhu, B. Xu and X. Wang, *Spectrosc. Spect. Anal.*, 2009, **29**, 3011.
31 M.J. Godinho, R.F. Gonçalves, L.P.S. Santos, J.A. Varela, E. Longo and E.R. Leite, *Mater. Lett.*, 2007, **61**, 1904.
32 Y. Hamlaoui, F. Pedraza, C. Remazeilles, S. Cohendoz, C. Rébéré, L. Tifouti and J. Creus, *Mater. Chem. Phys.*, 2009, **113**, 650.